Downloaded from SAE International by Universita degli Studi di Modena, Wednesday, October 08, 2025

2025-24-0015 Published 07 Sep 2025

Influence of Geometric Parameters on the Performance of TPMS-Based Heat Exchangers

Ilario Cordisco, Federico Torri, Fabio Berni, Veronica Testa, Mauro Giacalone, and Stefano Fontanesi Università di Modena e Reggio Emilia

Citation: Cordisco, I., Torri, F., Berni, F., Testa, V. et al., "Influence of Geometric Parameters on the Performance of TPMS-Based Heat Exchangers," SAE Technical Paper 2025-24-0015, 2025, doi:10.4271/2025-24-0015.

Received: 05 May 2025 Revised: 27 Jun 2025 Accepted: 27 Jun 2025

Abstract

Advancements in additive manufacturing (AM) technology have enabled the use of Triply Periodic Minimal Surface (TPMS) lattice structures to integrate thermal and structural functions into a single component. These structures offer advantages such as weight reduction, compactness and enhanced heat dissipation, making them promising for automotive, aerospace and electronics applications. TPMS structures, characterized by zero mean curvature and periodic crystalline geometry, have recently gained significant research attention thanks to their potential in thermal management. Among various TPMS geometries, the gyroid and diamond structures stand out for their thermal and fluid dynamic performance. This study explores the influence of cell geometry, unit cell size, and wall thickness on the efficiency of TPMS-based heat exchangers, as these parameters are crucial for their technical feasibility. Using Computational Fluid Dynamics (CFD) simulations, a comparative analysis is conducted for a case study represented by a heat exchanger. The numerical approach relies on a steady-state Reynolds-Averaged Navier-Stokes (RANS) approach with the Reynolds Stress Transport (RST) Elliptic Blending model, while heat transfer is analyzed through the Conjugate Heat Transfer (CHT) technique. The results indicate that reducing the unit cell size enhances heat transfer but also increases pressure drop at a fixed flow rate. Similarly, increasing the wall thickness raises pressure losses, though its effect on heat transfer is minimal. Overall, the diamond structure outperforms the gyroid in both thermal efficiency and flow permeability, making it a more effective choice for TPMS-based heat exchangers. These findings offer valuable insights for optimizing TPMS geometries in high-performance heat transfer applications, guiding future research and industrial implementations.

Introduction

A heat exchanger is a device aiming to transfer heat between two or more fluids without mixing them. They are fundamental in a vast range of applications, including power generation [1], heating, ventilation and air conditioning (HVAC) [2], waste heat recovery [3, 4], and thermal management for the automotive [5], aerospace [6] and electronics industries [7].

Given the broad range of applications, heat exchangers must be optimized for thermal performance, flow resistance, size, weight, and cost. In high-performance sectors, such as automotive and aerospace, the need for lightweight, compact, and efficient heat exchangers is critical. Structures that are interesting for the purpose are Triply Periodic Minimal Surfaces (TPMS) lattice ones. Although originally theorized by H. Schwarz in 1865, they have only recently gained significant attention inside the scientific community, thanks to the advancements in the additive manufacturing technology, which now makes it feasible to physically produce these complex geometries.

The most common AM technique for metal heat exchangers is the powder bed fusion (PBF) [8] which consists of a laser (or electron beam) selectively melting metal powder, layer by layer. Its main advantages are good mechanical properties of the printed parts and high resolution, which enables the production of thin walls and small channels. On the other hand, the structure could be affected by thermal residual stresses, and it could be difficult to clean the metal powder from intricate channels. Another technique for metal heat exchangers, but also for ceramic ones, is the binder jetting [9]. In this case, a liquid binder is jetted onto a powder bed to form a "green" part, which is then sintered. The process allows high production rates, and it is not affected by thermal residual stresses, but the resulting mechanical properties are usually poorer than PBF. Moving to polymer and composite heat exchangers, the fused filament fabrication (FFF) [10] enables the creation of lightweight, cost-effective designs, including novel structures with embedded metal fibers for improved thermal performance.

Downloaded from SAE International by Universita degli Studi di Modena, Wednesday, October 08, 2025

TPMS are mathematically defined surfaces that repeat periodically in three dimensions and are locally area-minimizing, offering structural strength, high surface-to-volume ratio, and interconnected flow paths. Additionally, TPMS structures can be highly customized through a wide range of design parameters, such as topology of the structure, periodic length in each direction, ratio between the volumes occupied by the fluids and wall thickness. This last parameter is particularly important because it is linked to the technological feasibility of the structure.

Many studies have been done on the optimization of TPMS-based heat exchangers by changing the aforementioned design variables.

R. Attarzadeh et al [11] used CFD to study a low temperature TPMS-based heat exchanger for a waste heat recovery system. The study case consisted in a channel filled with a Schwarz-D (Diamond) TPMS cube. On one side of the TPMS, a constant temperature plate represented the heat source. By changing the wall thickness of the structure, relationships were established between gas velocity, heat transfer and thermal performance of the heat exchanger. It was found that a smaller wall thickness resulted in higher thermal performance.

As a prosecution of that study, R. Attarzadeh et al. [12] proposed an automated workflow to perform a multi-objective optimization process of the heat exchanger, based on a Genetic algorithm (MOGA). The optimization targets were pressure drop minimization and temperature recover maximization of the flow through the heat exchanger by changing fluid properties, geometric parameters, and boundary conditions inside predetermined ranges. It was found that the thermal performance of the TPMS-based heat exchanger was extremely sensitive to wall thickness, pore diameter and periodic length of the TPMS. In particular, increasing wall thickness and/or reducing pore diameters or pattern length led to improved thermal performance of the heat exchanger.

R. Min et al. [13] constructed flexible hybrid TPMS structures, starting from original ones (primitive, gyroid, and diamond), by sigmoid transition parameters and analyzed their internal flow and heat transfer mechanisms in depth by means of CFD simulations. Additionally, the hybrid structures were also compared to the original ones, for a total of six tested topologies. The study case consisted of a cube of 40 mm x 40 mm x 40 mm made of aluminum TPMS cells with a 10 mm cell size, where two fluids (water) exchanged heat in a cross-flow configuration. The result showed that the Gyroid-Diamond TPMS heat exchanger had the highest heat exchange efficiency and convective heat transfer coefficient, but had also a relatively large pressure drop.

O. Abdelqader et al. [14] examined the structural architectures of TPMS to maximize the generation of freshwater from moist air under various humidity and flow conditions, by employing accurate 3D CFD models. They compared the freshwater production efficiency of various TPMS designs (Gyroid-Solid, Gyroid-Sheet, and Diamond-Solid) against a vertical flat plate with the same surface area. The findings indicated that the Diamond-Solid structure exhibited superior performance when subjected to low airflow Reynolds numbers, whereas at high Reynolds numbers the Gyroid-Sheet exhibited the highest level of condensation among the three structures. In general, the condensation flow rate was increased by three times compared to the flat plane across various levels of humidity in the air.

In a following study, O. Abdelqader et al. [15] extended the previous comparison to various tube shapes and orientations, including smooth and finned surfaces, as well to the IWP TPMS structure, keeping the same surface area across each geometry. The findings revealed that horizontally oriented tubes (i.e. the tube axis is perpendicular to the air flow) outperform vertical ones, primarily due to their larger length-to-diameter ratio and fin alignment. The Gyroid-Solid structure demonstrated a 40% increase in water production compared to the best tubular configuration, while the IWP-Solid structure produced 10% more. The Gyroid-Sheet and IWP-Sheet structures condensed less water than the finned tube at low Reynolds numbers. However, at higher Reynolds numbers, the Gyroid-Sheet outperformed the finned tube by enhancing flow turbulence, with the IWP-Sheet structure yielding comparable results.

N. Song et al. [16] designed a heat exchanger based on a Gyroid-type TPMS structure according to the actual working conditions of fuel/lubricating oil heat exchangers in an aero-engine. Numerical simulations were conducted to study the relationship between three design parameters (uniform lattice size, unidirectional lattice size, and hot/cold fluid porosity ratio) and the key characteristics of the heat exchanger, such as the flow resistance and the convective heat transfer. They found out that decreasing the lattice size, especially in the direction of the flow, improved the heat transfer effect by increasing the heat exchange area. Additionally, changing the distribution of the hot and cold fluid channels, by using a double porosity for the former, resulted in the best convective heat transfer coefficients in the range of tested values.

H. C. Wang et al. [17] designed a crossflow heat exchanger, between hot air and cold aviation kerosene, equipped with a Gyroid TPMS structure. They studied the effects of volume and flow rate distribution, among hot and cold fluids, on the performance. Based on numerical simulations, and considering the simultaneous pressure drop penalty, lower flow rate and volume were recommended for the cold fluid to improve the thermal performance. In addition to that, the Gyroid heat exchanger provided a significant improvement of approximately an order of magnitude in the volume-based power density and normalized pressure drop compared to typical heat exchanger configurations.

F. Torri et al. [18] compared four TPMS structures, namely Gyroid, I-WP, Primitive, and Diamond, and a traditional plate heat exchanger in terms of heat transfer and pressure drop by means of 3D-CFD simulations. The structures were compared considering equal volume of the specimen, wall thickness, and unit cell dimension. It was found that the Diamond structure outperformed the others in terms of heat transfer, while the Primitive had

Downloaded from SAE International by Universita degli Studi di Modena, Wednesday, October 08, 2025

the smallest pressure drop. Each tested TPMS structure offered better heat transfer, and more pressure drop than the plate heat exchanger with turbulators.

To summarize the key findings of the discussed literature review, heat transfer maximization and pressure drop minimization were contrasting optimization targets across almost all applications. Changing the design variables of the TPMS structures had an enormous impact on the performance of the heat exchangers, which were consistently able to outperform traditional solutions. Nevertheless, the selection of the design variables is strongly dependent on the particular application.

Given the little amount of research on the topic, this study analyses the particular case of an automotive application for TPMS structures, considering a cross-flow heat exchanger with water and engine lubricant oil as working fluids. For this application, especially for high-end and racing vehicles, it is important to create a heat exchanger with high power density to minimize size and mass. Indeed, this is a way to free space for other devices and to efficiently cool down the lubricant oil. On the other hand, pressure drops through the heat exchanger are important for the design of the hydraulic circuits, therefore they need to be kept as low as possible. As already said, thermal and fluid dynamic performances are contrasting design targets. Consequently, it is interesting to evaluate the effect of the main TPMS design variables on the performance of the heat exchanger.

This study investigates, by means of 3D-CFD simulations, the effect of unit cell size and wall thickness on the heat exchanger performance, considering two of the most promising TPMS structures for similar applications, namely Diamond and Gyroid. The aim of this work is to give insight into the design process of TPMS-based heat exchangers for automotive applications.

Methodology

Main Parameters for the Analysis of TPMS-Based Heat Exchangers

TPMS can be defined by implicit algebraic equation in the form of Equation 1.

$$f(\boldsymbol{r}) = \sum_{k=1}^{N} A_k \cos\left[\frac{2\pi(\boldsymbol{h}_k \cdot \boldsymbol{r})}{\lambda_k} + P_k\right] = C \tag{1}$$

A_k is the amplitude, $\boldsymbol{h}_k$ is the k^{th} lattice vector in the reciprocal space, $\boldsymbol{r}$ is the location vector, λ_k is the period factor, P_k is the function phase and C is the curvature parameter. Based on that, the Diamond (D) and the Gyroid (G) structures visible in Figure 1 are defined by Equations 2 and 3, respectively.

$$f(x,y,z) = \cos(\omega_x x)\cos(\omega_y y)\cos(\omega_z z) + -\sin(\omega_x x)\sin(\omega_y y)\sin(\omega_z z) = C \tag{2}$$

FIGURE 1 Unit cells of (a) Diamond and (b) Gyroid, showing the solid, hot fluid, and cold fluid domains. *l* is the unit cell size.

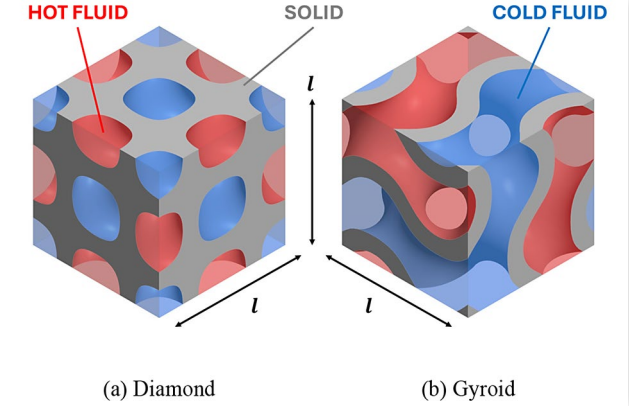

$$f(x,y,z) = \sin(\omega_x x)\cos(\omega_y y) + \sin(\omega_z z)\cos(\omega_x x) + \sin(\omega_y y)\cos(\omega_z z) = C \tag{3}$$

ω_i is the periodic parameter in the *i*-direction and, in this study, it is equal in each of the three directions, because only uniform TPMS are considered (i.e. the unit cell is cubic). If different periodic parameters are used in the three directions, the resulting unit cell is not a cube, but a general parallelepiped. On the other hand, the curvature parameter C controls the wall thickness and, consequently, the structure porosity ϕ, defined as in Equation 4.

$$\phi = \frac{V_f}{V_{cell}} = \frac{V_f}{V_s + V_f} \tag{4}$$

V_{cell} is the volume of the unit cell (i.e. the volume of a cube of side l, corresponding to the unit cell size), V_f is the volume occupied by the fluids and V_s is the volume occupied by the solid wall. In this regard, the solid wall is generated by equally offsetting the TPMS in both directions, and it divides the cell into two immiscible fluid channels.

The wall thickness is incredibly important for the technological feasibility of TPMS structures, especially when they are used as heat exchangers. Indeed, deviations from the nominal shape during the additive manufacturing process can result in holes through the solid wall, especially when it is very thin, making the system unable to operate as heat exchanger. Therefore, in most cases, a minimum wall thickness is imposed by the manufacturing technology. Moreover, a design constraint on the minimum wall thickness could also be imposed by structural considerations.

Given the importance, it is useful to correlate the wall thickness with the porosity and the wall surface area of the structure. This is relevant because the porosity is linked to the flow resistance inside the channels and the wall surface area is related to the heat transfer between

Downloaded from SAE International by Universita degli Studi di Modena, Wednesday, October 08, 2025

the fluids. A correlation between all these aspects gives information on the interaction between technological, structural, fluid dynamic and heat transfer properties of the structure.

In this study, such correlations are done by generating different TPMS structures with the MATLAB software MSLattice [19] and then measuring their geometrical properties inside a CAD environment. In order to keep a general approach, the wall thickness (t) and the heat exchange surface area (A_{wall}) are expressed in dimensionless terms, exploiting their relationship with the unit cell size l. Hence, the relative wall thickness t_r and the relative wall surface area $A_{wall,r}$ are defined as in Equations 5 and 6, respectively.

$$t_r = \frac{t}{l} \tag{5}$$

$$A_{wall,r} = \frac{A_{wall}}{l^2} \tag{6}$$

The correlation between structure porosity and relative wall thickness for Diamond and Gyroid are shown in Figure 2. As a first approximation, the volume occupied by the solid wall is equal to the wall surface area times the wall thickness. Therefore, the relative wall thickness should be inversely proportional to the structure porosity, which is the case for both geometries when the porosity is high. On the contrary, for low levels of porosity, the behavior is non-linear, especially for the Gyroid structure.

Comparing Diamond and Gyroid, the former always has a lower porosity, for each value of relative wall thickness. If the porosities of both geometries are equal, the relative wall thickness of the Diamond is always lower than the Gyroid one, which suggests that the Diamond has a greater relative wall surface area than the Gyroid. Indeed, as shown in Figure 3, that is the case. In an ideal scenario with an infinitely thin wall, the relative wall surface area of the Diamond is 7.68, while it is 6.18 for the Gyroid, suggesting a better heat transfer performance for the first one. Those values decrease when the porosity is reduced, until they obviously reach zero for a null porosity (i.e., the unit cell is completely made of solid, so there are not fluid channels).

FIGURE 2 Correlation between relative wall thickness and porosity for the Diamond and Gyroid structures.

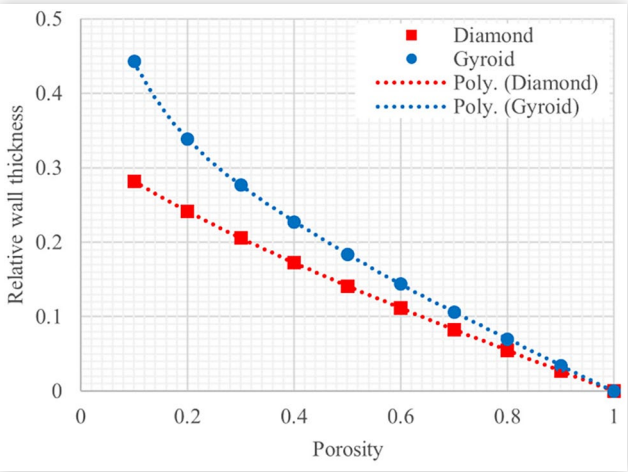

FIGURE 3 Correlation between relative wall surface area and porosity for Diamond and Gyroid structures.

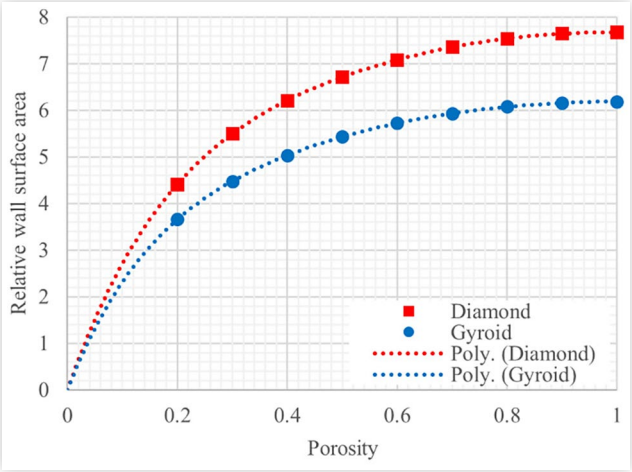

Both relative wall thickness and relative wall surface area are dependent on the porosity. Hence, it is possible to relate them directly, as it is shown in Figure 4. For both the structures, when the relative wall thickness is increased, the wall surface area decreases. As already said, the Diamond has more relative surface area than the Gyroid, but it loses surface area faster with increasing wall thickness, completely losing its advantage when the relative wall thickness reaches 0.22. This suggests that the Diamond is more sensible than the Gyroid to wall thickness variations.

In this study, a fixed heat exchange volume filled with a TPMS structure is considered. Therefore, when the unit

FIGURE 4 Correlations between relative wall surface area and relative wall thickness for the investigated Diamond and Gyroid structures.

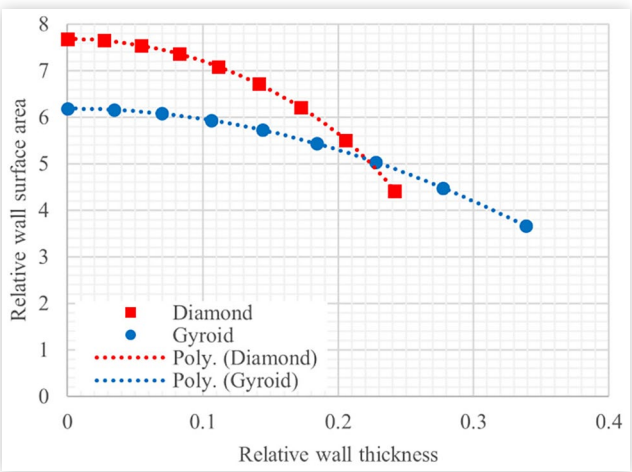

Downloaded from SAE International by Universita degli Studi di Modena, Wednesday, October 08, 2025

cell size changes, the number of cells that occupy the volume changes as well. That has no effect on the porosity of the structure because it only depends on the relative wall thickness. Nevertheless, if a certain wall thickness must be maintained for technological reasons, changing the unit cell size implies a variation of relative wall thickness and, thus, porosity.

For what concerns the heat transfer characteristics of the structures, an important parameter is the area-to-volume ratio S_V, defined as in Equation 7.

$$S_V = \frac{NA_{wall}}{V_{tot}} = \frac{NA_{wall}}{NV_{cell}} = \frac{A_{wall,r}(\phi)l^2}{l^3} = \frac{A_{wall,r}(\phi)}{l} \quad (7)$$

N is the number of TPMS cells contained in a fixed volume V_{tot}. This parameter is important because it represents the heat transfer area per unit of volume and, consequently, it determines the heat transfer for a given volume of heat exchanger.

As already said, the relative wall surface area is a function of the relative wall thickness of the structure. Therefore, the area-to-volume ratio depends on both the unit cell size and the wall thickness of the structure.

In this study, the attention is focused on TPMS structures with a unit cell size spanning from 5 mm to 12 mm and on a wall thickness in the range between 0.5 mm to 1.0 mm. Porosity and area-to-volume ratios for Diamond and Gyroid structures in the ranges of unit cell size and wall thickness presented above are proposed in Figure 5. It can be noted that the Diamond shows less porosity than the Gyroid, suggesting a higher resistance to the flow. On the other hand, the Diamond has also a higher area-to-volume ratio, which is an indicator of greater heat transfer.

The study case consists in a cross-flow heat exchanger (Figure 6) made by a TPMS lattice structure of aluminum, which occupies a volume defined by a square base with side of 36 mm (L_1) and a height equal to the unit cell size (l). The base is surrounded by a 7 mm layer of aluminum, which isolates the TPMS structure from the outside, and it presents small straight channels to consent both fluids to move inside the heat exchanger volume without mixing. In this way, the solid is confined inside a 50 mm (L_2) square base. In addition to that, both fluids enter and exit the heat exchanger through pipes of rectangular section ($L_1 \cdot l$) and 20 mm length (L_3). Ideally, the study case aims to represent a single cell "slice" of a larger heat exchanger of height 36 mm (50 mm considering the outer solid).

Such case study is interesting for high-end applications in automotive, aerospace, and electronics. The working fluids employed in this study are water at 50°C and engine oil at 80°C, which are typical testing temperatures for this automotive applications [20]. Properties of fluids and solid are presented in Table 1.

For what concern the flow rates, Table 2 shows the adopted values. In particular, the investigated flow rates are obtained scaling the ones of a conventional device used in a high-performance automotive application. The scaling factor is the ratio between the section area of the

FIGURE 5 Porosity and area-to-volume ratios of Diamond and Gyroid structures as a function of unit cell size and wall thickness.

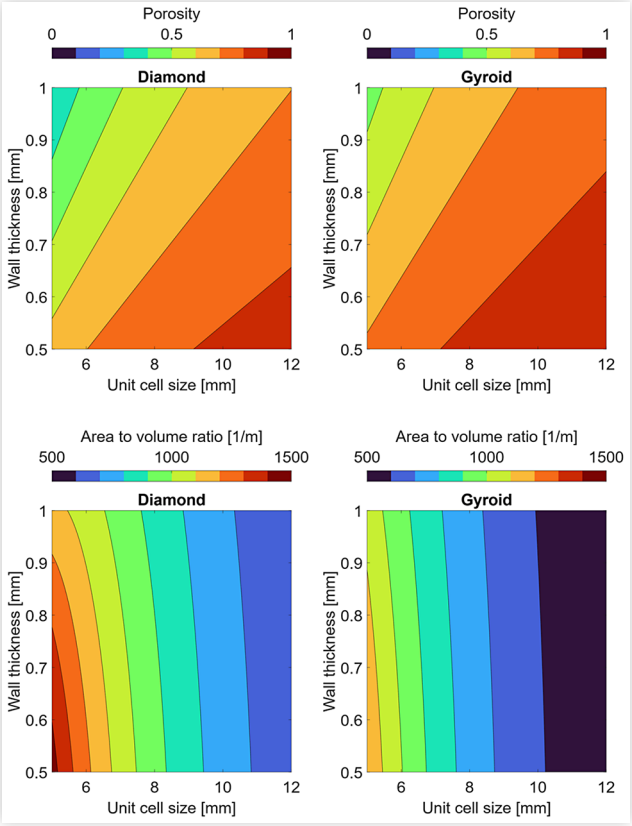

FIGURE 6 Simulation domain. It represents a "slice" of height l of a larger heat exchanger.

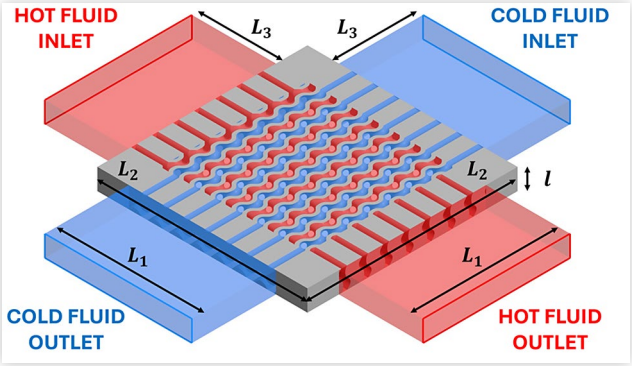

TABLE 1 Material properties.

Property	Unit	Oil	Water	AlSi10Mg
Temperature T	°C	80	50	-
Density ρ	kg/m^3	794.8	988.0	2702.0
Dynamic viscosity μ	mPa s	18.620	0.547	-
Specific heat capacity c_p	J/kg K	1992	4180	903
Thermal conductivity κ	W/m K	0.138	0.644	115
Prandtl number $Pr = \mu c_p/\kappa$	-	268.77	3.55	-

Downloaded from SAE International by Universita degli Studi di Modena, Wednesday, October 08, 2025

TABLE 2 Flow rates and corresponding inlet velocities for the complete heat exchanger (i.e. not for a single cell "slice", but for the entire cube).

Case	Hot oil flow rate complete heat exchanger l/min	Hot oil inlet velocity m/s	Cold water flow rate complete heat exchanger l/min	Cold water inlet velocity m/s
1	9.5	0.122	15	0.193
2	13	0.167	20	0.257
3	16	0.206	25	0.322
4	19	0.244	30	0.386

case study and that of the conventional exchanger, which can not be provided due to confidentiality reasons.

To address fluid dynamic and thermal properties of the heat exchanger, it is useful to introduce some important parameters. One of them is the Reynolds number *Re*, defined as in Equation 8.

$$Re_i = \frac{\rho_i v_i D_i}{\mu_i} \tag{8}$$

ρ_i is the fluid density, v_i is a reference velocity, D_i is a characteristic length for the problem and μ_i is the dynamic viscosity of the fluid, all referred to the *i*-fluid.

For the present study, the average velocity inside the channels can be used as reference. Since a TPMS structure can be considered as a porous media, the superficial velocity formulation can be used to calculate the average velocity inside the channels, reported in Equation 9.

$$v_i = \frac{2v_{s,i}}{\phi} = \frac{v_{s,i}}{\phi_i} \tag{9}$$

$v_{s,i}$ is the superficial velocity, ϕ is the porosity of the TPMS structure and ϕ_i is the porosity associated to one fluid phase. In this regard, $\phi_i = \phi/2$ because it is the volume occupied by one of two identical fluid channels divided by the cell volume (l^3). It is useful to exploit the superficial velocity because it is proportional to the flow rate inside the heat exchanger, which is often a design constraint. On the other hand, the average velocity inside the TPMS structure depends on its dimensions and topology, which are tunable parameters.

To complete the definition of the Reynolds number, the hydraulic diameter is expressed as in Equation 10.

$$D_h = \frac{4V_f}{A_{wall}} = \frac{4\phi V_{cell}}{A_{wall}} = \frac{4\phi l^3}{A_{wall,r}(\phi) l^2} = \frac{4\phi}{S_V} \tag{10}$$

This is similar to the definition of hydraulic diameter for non-circular pipes, which is four times the section area divided by the wetted perimeter.

Substituting (9) and (10) inside (8), the Reynolds number can be written as in Equation 11.

FIGURE 7 Reynolds numbers of water and oil as a function of unit cell size and wall thickness for Diamond and Gyroid structures.

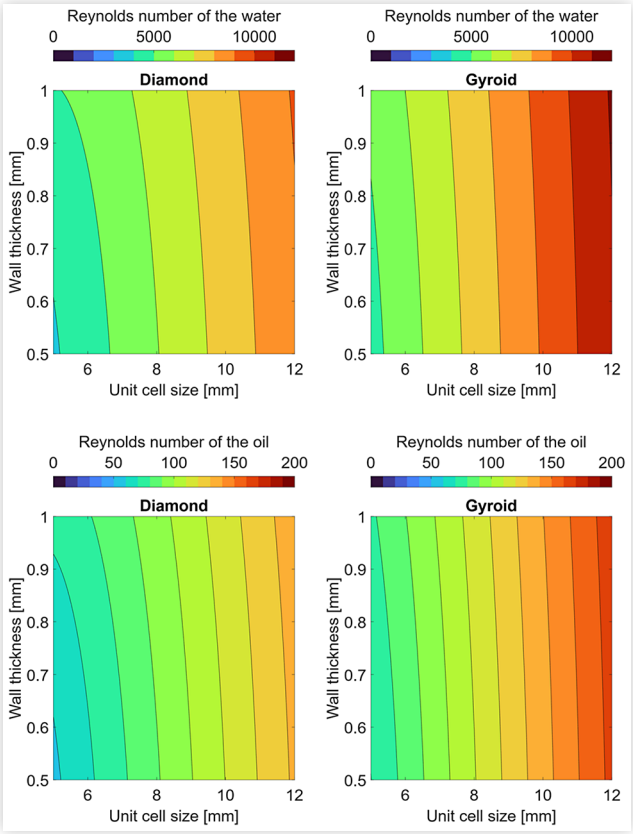

$$Re_i = \frac{8\rho_i v_{s,i} l}{\mu_i A_{wall,r}(\phi)} = \frac{8\rho_i v_{s,i}}{\mu_i S_V} \tag{11}$$

Using this definition and considering the maximum superficial velocities of oil and water tested in this study (reported in Table 2), it is possible to estimate the Reynolds numbers of both the fluids for each combination of TPMS structure, unit cell size, and wall thickness, as it is shown in Figure 7.

The heat transfer of each fluid can be calculated as:

$$Q_i = c_{p,i} m_i \left| T_{out,i} - T_{in,i} \right| \tag{12}$$

$c_{p,i}$ is the specific heat at constant pressure, m_i is the mass flow rate, $T_{out,i}$ is the outlet temperature, and $T_{in,i}$ is the inlet temperature, all referring to the *i*-fluid. In the numerical simulations, the heat loss between hot and cold fluids is negligible, therefore the heat transfer can be defined by averaging the heat transfer of hot and cold fluids (that, as obvious, are almost coincident), following Equation 13.

$$Q = \frac{Q_{cold} + Q_{hot}}{2} \tag{13}$$

The convective heat transfer coefficient of each fluid is defined as in Equation 14.

Downloaded from SAE International by Universita degli Studi di Modena, Wednesday, October 08, 2025

$$h_{conv,i} = \frac{Q_i}{A_{wall}\left|T_{wall,i} - T_i\right|} \tag{14}$$

A_{wall} is the TPMS wall surface area, $T_{wall,i}$ is the average temperature of the *i*-fluid on the corresponding TPMS wall and T_i is the average temperature of the *i*-fluid, calculated as the average between the inlet and outlet temperatures.

The conductive heat transfer coefficient through the solid walls is computed by Equation 15.

$$h_{cond} = \frac{Q}{A_{wall}\left|T_{wall,hot} - T_{wall,cold}\right|} \tag{15}$$

From the heat transfer coefficients, it is possible to define the corresponding thermal resistances as in Equation 16.

$$R_i = \frac{1}{h_i}; \tag{16}$$

The global heat transfer coefficient *U* or the total thermal resistance *R* are obtained by solving Equation 17.

$$R = R_{conv,hot} + R_{conv,cold} + R_{cond} = \frac{1}{U} \tag{17}$$

In order to characterize the convective heat transfer, an important dimensionless parameter is the Nusselt number, defined by Equation 18.

$$Nu_i = \frac{h_{conv,i} D_h}{\kappa_i} \tag{18}$$

κ_i is the thermal conductivity of the *i*-fluid.

The resistance of the fluid flow through the TPMS structures is analyzed through the Darcy friction factor, defined as in Equation 19.

$$f_i = \frac{2\Delta p_i D_h}{\rho_i L_1 v_i^2} \tag{19}$$

Δp_i is the pressure drop and L_1 is the length of the TPMS heat transfer volume in the direction of the flow, both referred to the *i* - fluid.

Additionally, it is also useful to consider the pumping power required by the fluids to flow through the heat exchanger. The total pumping power is defined as the sum of the water and oil contributes as in Equation 20.

$$P_{pump,tot} = P_{pump,w} + P_{pump,o} = \dot{V}_w \Delta p_w + \dot{V}_o \Delta p_o \tag{20}$$

$\dot{V}_w$ is the water volumetric flow rate, $\dot{V}_o$ is the oil volumetric flow rate, Δp_w is the water pressure drop, and Δp_o is the oil pressure drop.

Computational Fluid Dynamics Simulation Framework

The flow inside the heat exchanger is investigated by means of CFD simulations, which are conducted by the commercial software STAR-CCM+ [21] using three-dimensional steady-state RANS equations, including continuity and momentum equations reported in Equations 21 and 22, respectively.

$$\nabla \cdot \left(\rho \mathbf{v}\right) = 0 \tag{21}$$

$$\frac{\partial\left(\rho \mathbf{v}\right)}{\partial t} + \nabla \cdot \left(\rho \mathbf{v} \otimes \mathbf{v}\right) = -\nabla \cdot \left(p\mathbf{I}\right) + \nabla \cdot \mathbf{T} + \mathbf{f}_b \tag{22}$$

ρ is the density, $\mathbf{v}$ is the velocity, p is the pressure, $\mathbf{I}$ is the identity tensor, $\mathbf{T}$ is the viscous stress tensor, $\mathbf{f}_b$ is the resultant of the body forces acting on the continuum and $\otimes$ denotes the outer product.

Heat transfer is considered by the energy equation that, for a fluid in steady conditions, is written in the integral form proposed in Equation 23.

$$\oint_A \rho H \mathbf{v} \cdot d\mathbf{a} = -\oint_A \dot{\mathbf{q}}'' \cdot d\mathbf{a} + \oint_A \mathbf{T} \cdot \mathbf{v} d\mathbf{a} + \int_V \mathbf{f}_b \cdot \mathbf{v} dV + \\ + \oint_A \sum_i h_i J_i d\mathbf{a} + \int_V S_u dV \tag{23}$$

For a static solid in steady conditions, it is written as in Equation 24.

$$\oint_A \dot{\mathbf{q}}'' \cdot d\mathbf{a} = \int_V S_u dV \tag{24}$$

H is the total enthalpy, $\dot{\mathbf{q}}''$ is the heat flux, h_i is the enthalpy of *i*-component, J_i is the diffusive flux of *i*-component and S_u is a user-specified source term.

On the interface between fluid and solid, a Conjugate Heat Transfer (CHT) problem must be solved to conserve the total heat flux (as well as the energy) across the interface.

Based on the available research on the topic, the Reynolds Stress Transport (RST) with Elliptic Blending [22] is selected as turbulence model.

The Reynolds Stress Transport (RST) turbulence model in the Elliptic Blending version [23] can consider the effect of turbulence anisotropy, the curvature of the streamlines and the swirl motion, thus being potentially more accurate than Eddy Viscosity models. RST models directly compute the components of the Reynolds Stress tensor by solving the transport equations resumed by Equation 25.

$$\frac{D\left(\overline{u_i u_j}\right)}{Dt} = P_{ij} + \phi_{ij}^* - \varepsilon_{ij} + D_{ij}^t + \frac{\partial}{\partial x_k}\left(\nu \frac{\partial\left(\overline{u_i u_j}\right)}{\partial x_k}\right) \tag{25}$$

Downloaded from SAE International by Universita degli Studi di Modena, Wednesday, October 08, 2025

P_{ij} is the turbulent production, ϕ_{ij}^{*} is the pressure-strain, ε_{ij} is the turbulent dissipation-rate, and D_{ij}^{t} is the turbulent diffusion. As opposed to the two equations of the Eddy Viscosity models, seven equations must be solved for an RST model: six equations for the Reynolds stresses (i.e. one for each component of the Reynolds stress symmetric tensor) and one for the isotropic turbulent dissipation-rate ε. Consequently, RST models are more computationally expensive than Eddy Viscosity ones.

The main difference between RST models lies in the definition of the pressure strain ϕ_{ij}^{*}. The Elliptic Blending RST model is based on a blending of near-wall and weakly inhomogeneous models for pressure-strain and dissipation terms, as shown in Equation 26.

$$\phi_{ij}^{*} - \varepsilon_{ij} = \left(1-\alpha^{3}\right)\left(\phi_{ij}^{w} - \varepsilon_{ij}^{w}\right) + \alpha^{3}\left(\phi_{ij}^{h} - \varepsilon_{ij}^{h}\right) \tag{26}$$

w refers to the near-wall formulation, h to the weakly inhomogeneous formulation and α is a blending parameter, which is the solution of the elliptic equation presented in Equation 27.

$$\alpha - L^{2}\nabla^{2}\alpha = 1 \tag{27}$$

The length-scale L is defined as in Equation 28.

$$L = C_{l} max\left(\frac{k^{3/2}}{\varepsilon}, C_{\eta}\frac{\nu^{3/4}}{\varepsilon^{1/4}}\right) \tag{28}$$

C_l and C_η are model coefficients, k is the turbulent kinetic energy, ε is the turbulent dissipation-rate, and ν is the kinematic viscosity of the fluid.

All simulations employ segregated solvers with SIMPLE algorithm for the pressure-velocity coupling. Flow and energy equations are solved with second-order differencing schemes.

As already said, the hot fluid is engine lubricant oil at 80°C and the cold fluid is water at 50°C. Temperatures and velocities are imposed at the inlets, while ambient pressure is imposed at the outlets. Both fluids enter the domain with a turbulence intensity of 5% and a turbulent length scale of one tenth of the unit cell size. The inlet velocities of the heat exchanger "slice" correspond to four combinations of oil and water flow rates across the complete heat exchanger of height L_1 (Table 2), which are of interest for the application studied in this work. Since only a "slice" of the heat exchanger is considered, upper and lower surfaces are treated as periodic boundaries. In this way, the vertical periodicity of the structure is considered. The interfaces between solid and fluid are associated with no-slip conditions, and they can be crossed by heat fluxes, while all the remaining surfaces are adiabatic walls.

The stopping criteria of the simulations are based on the convergence of pressure drops, outlet temperatures, and heat transfer, which represent the investigated quantities.

Mesh Sensitivity Analysis

To discretize and solve the governing equations, the fluid and solid domains are meshed with polyhedral cells of uniform size. In addition to that, prismatic layers are employed on the fluid side of the fluid-solid interfaces to adequately capture the turbulent and thermal boundary layers (Figure 8). For the selection of the mesh parameters, particularly those of the prismatic layers, a low Reynolds approach (i.e. targeting y^{+}~1) is adopted.

It is well known that grid resolution is one of the main factors affecting the results of a CFD simulation, therefore a mesh sensitivity analysis is required. The procedure consists in simulating the water flow inside one TPMS cell and gradually refining the mesh until the pressure drop stabilizes around a grid-independent value. As initial attempt, for each structure, a uniform mesh size equal to 1/20 of the TPMS unit cell size l is used for the whole domain, then that value is gradually reduced while the prismatic layers are iteratively adjusted to keep a reasonable expansion rate and an average y^{+} around one. After that, the parameters of the coarsest mesh that gives a result close to the grid-independent value are used to generate the mesh of the complete domain of the heat exchanger "slice", as shown in Figure 9. In general, the

FIGURE 8 Selected mesh for the Gyroid with 6 mm unit cell size and 0.75 mm of wall thickness on a single cell.

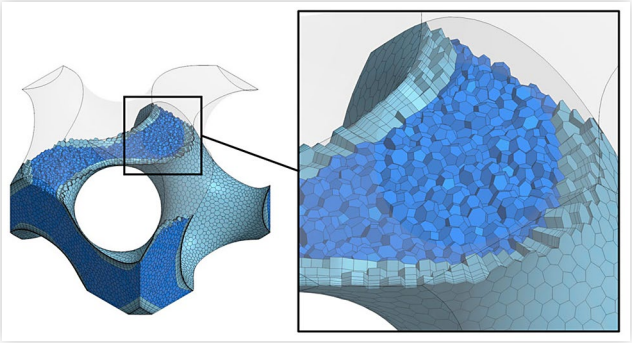

FIGURE 9 Selected mesh for the Gyroid with 6 mm unit cell size and 0.75 mm of wall thickness applied to the whole simulation domain.

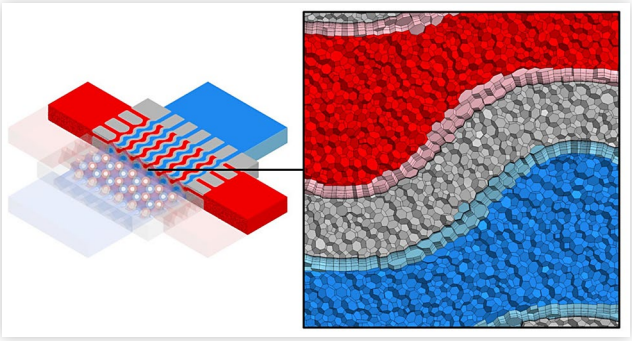

Downloaded from SAE International by Universita degli Studi di Modena, Wednesday, October 08, 2025

selected grids have a mesh size between 1.5% and 3.5% of the unit cell size *l*, a near wall prismatic layer thickness between 3.0 μm and 10.0 μm, a stretch factor between 1.47 and 2.00, a number of prismatic layers between 6 and 8, and a number of cells between 32˙694 and 150˙994. More details are presented in Appendix A.

The mesh sensitivity analysis is conducted only for the water channel of a single TMPS cell to reduce the computational cost required for this phase. In fact, the number of mesh cells needed for the whole domain ("slice", including inlet and outlet ducts) are roughly two hundred times higher than those of a single TPMS cell. To simulate a single cell, the boundary conditions of the simulation must be changed to consider the triply periodic behavior of the geometry, as described by Figure 10. Therefore, all the surfaces that the fluid can cross are treated as periodic interfaces, for a total of three, one for each direction. In detail, it guarantees the same velocity field on both sides of the interface. In the flow direction, the "fully-developed" option is used, which allows to fix a mass flow rate through the interface. This results in a pressure drop in the flow direction. For the other interfaces, both pressure and velocity fields are equal on the opposed surfaces.

The choice of simulating the water channel over the oil channel for the mesh selection procedure is a consequence of the higher Reynolds number associated with water, as previously shown in Figure 7. Indeed, water moves through the TPMS faster and it has a much lower viscosity than oil. Therefore, it is the fluid which is more likely to develop complex flow structures and, consequently, a grid able to predict its pressure drop is assumed to be a reasonable choice also for the oil and solid domain. To capture the flow behavior in the most complex scenario, the mesh sensitivity analysis is always performed using the highest water inlet velocity (0.386 m/s). Moreover, to further reduce the computational effort, only the cells with 0.75 mm of wall thickness are tested in this phase, because the Reynolds number is much more sensitive to the unit cell size rather than wall thickness. Then the optimal mesh found for a specific cell size is used for all the wall thicknesses.

FIGURE 10 Unit cell simulation domain used for the mesh sensitivity analysis. The external boundaries are periodic.

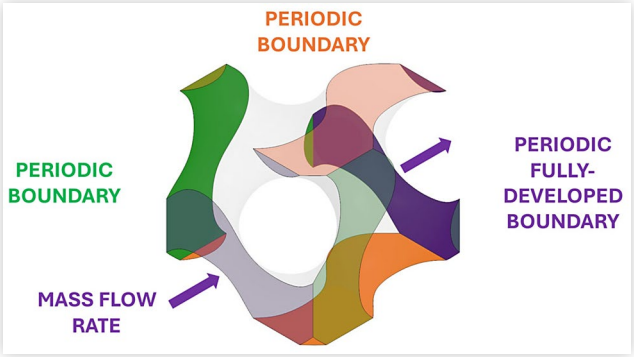

Results

Given the mesh sensitivity analysis and considering the validation of the adopted numerical framework carried out by Torri et al. [18] against the experimental data of Dixit et al. [24], simulations of different TPMS topologies, unit cell sizes, wall thickness, and flow rates were conducted to investigate their effects on the thermo-fluid dynamic performance of the water-oil heat exchanger.

Starting from pressure drops, results are shown in both Figure 11 for the water side and Figure 12 for the oil one. In those figures and in the following ones, unit cell size and wall thickness are referred in the legend as *l* – *t* (e.g. 5 – 0.50 means that the unit cell size is 5 mm and the wall thickness is 0.50 mm). The pressure drop always increases when the unit cell size is reduced, and the wall thickness is increased. Indeed, in both situations, the porosity of the heat exchanger decreases, leading to more flow resistance. To better explain this point, it is useful to rearrange the Darcy equation as in Equation 29, by introducing Equations 7, 9 and 10.

$$\Delta p_i = f_i \rho_i \frac{v_i^2}{2} \frac{L_1}{D_h} = f_i \rho_i \frac{v_{s,i}^2 S_V}{8\phi^3} L_1 = f_i \rho_i \frac{v_{s,i}^2 A_{wall,r}(\phi)}{8\phi^3 l} L_1 \qquad (29)$$

When the wall thickness is increased, the porosity ϕ decreases almost linearly, as described in Figure 2 (i.e. $\phi \cong 1 - kt/l$ where k is a constant value less than 1), while the cell relative surface area $A_{wall,r}(\phi)$ decreases much more slowly. Considering a constant flow rate through the heat exchanger (i.e., the superficial velocity $v_{s,i}$ is constant), the pressure drop is proportional to $1/\phi^3 l$ and, consequently, to $1/l(1 - kt/l)^3$, which increases with the wall thickness and decreases with the unit cell size.

Considering the same unit cell size and wall thickness, the Diamond geometry manifests higher pressure drops than the Gyroid. Indeed, in the ranges of unit cell size and wall thickness analyzed in this study, the Diamond has less porosity and more relative surface area than the Gyroid, which explains the higher pressure drops.

When the flow rate is increased, water and oil have different behaviors. For example, it is possible to analyze the Diamond structure with 5 mm of unit cell size and 0.75 mm wall thickness. When the water flow rate is doubled from 15 l/min to 30 l/min, the pressure drop changes from 20,723 Pa to 74,225 Pa, which is almost four times higher. This suggests that the flow is close to being fully turbulent. On the other hand, when the oil flow rate is doubled from 9.5 l/min to 19 l/min, the pressure drop increases from 30,081 Pa to 72,295 Pa, which is 2.4 times higher. Therefore, the oil is almost laminar. These findings suggest that, in a water-oil heat exchanger for automotive applications, the flow is likely to be in a transition zone between laminar and turbulent regimes for both fluids, with oil mostly laminar and water mostly turbulent. To give more details, Figure 13 and Figure 14 show the Darcy friction factor (given by Equation 19) plotted against the Reynolds number, for water and oil, respectively.

Downloaded from SAE International by Universita degli Studi di Modena, Wednesday, October 08, 2025

FIGURE 11 Water pressure drops for different TPMS topologies, unit cell sizes, and wall thicknesses. Legend: unit cell size *l* [mm] – wall thickness *t* [mm].

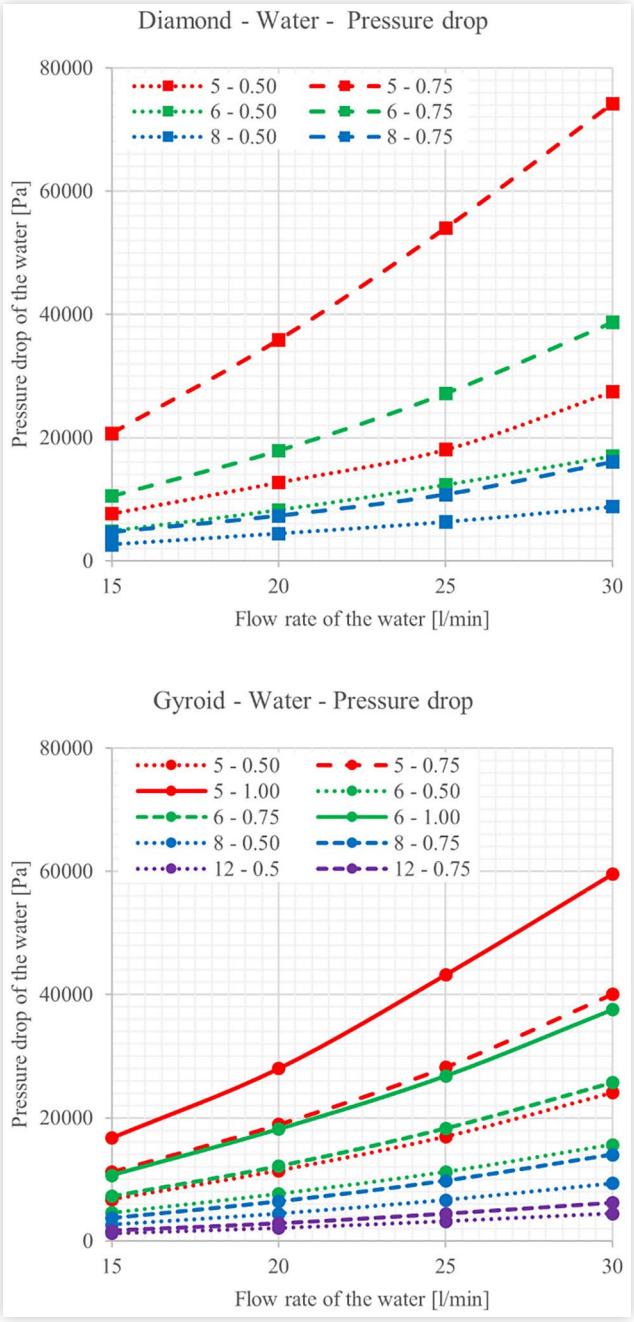

FIGURE 12 Oil pressure drops for different TPMS topologies, unit cell sizes, and wall thicknesses. Legend: unit cell size *l* [mm] – wall thickness *t* [mm].

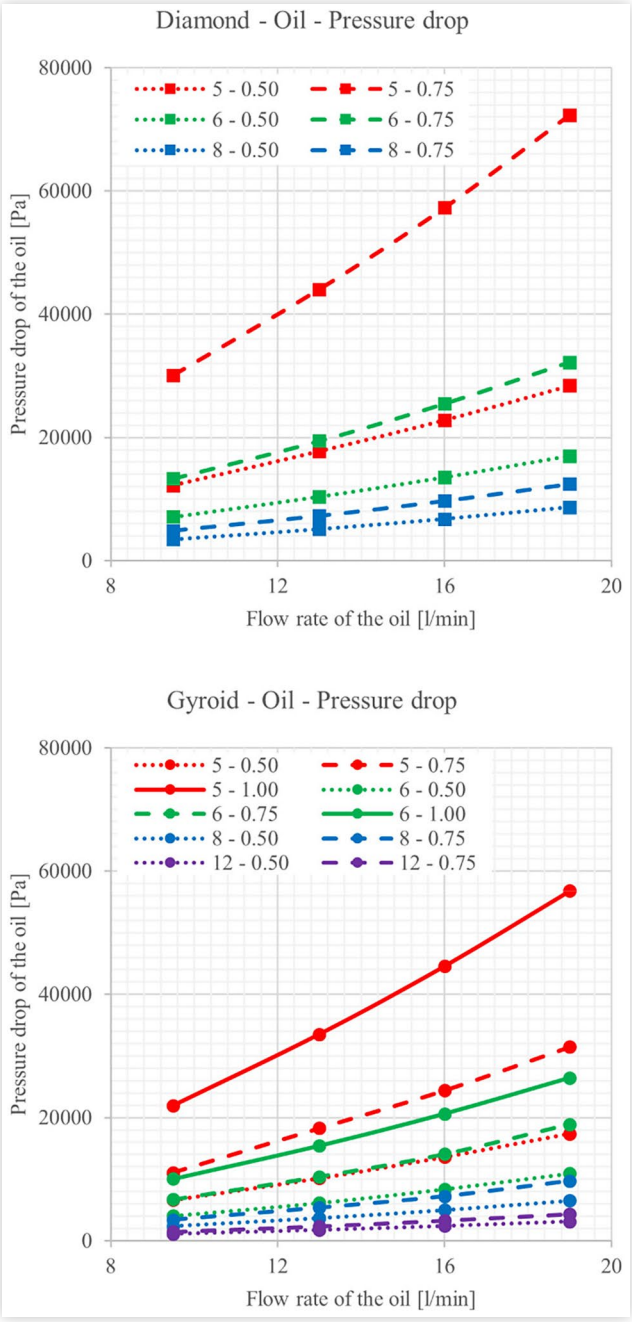

Downloaded from SAE International by Universita degli Studi di Modena, Wednesday, October 08, 2025

FIGURE 13 Darcy friction factor of water for different TPMS topologies, unit cell sizes and wall thicknesses. Legend: unit cell size *l* [mm] – wall thickness *t* [mm].

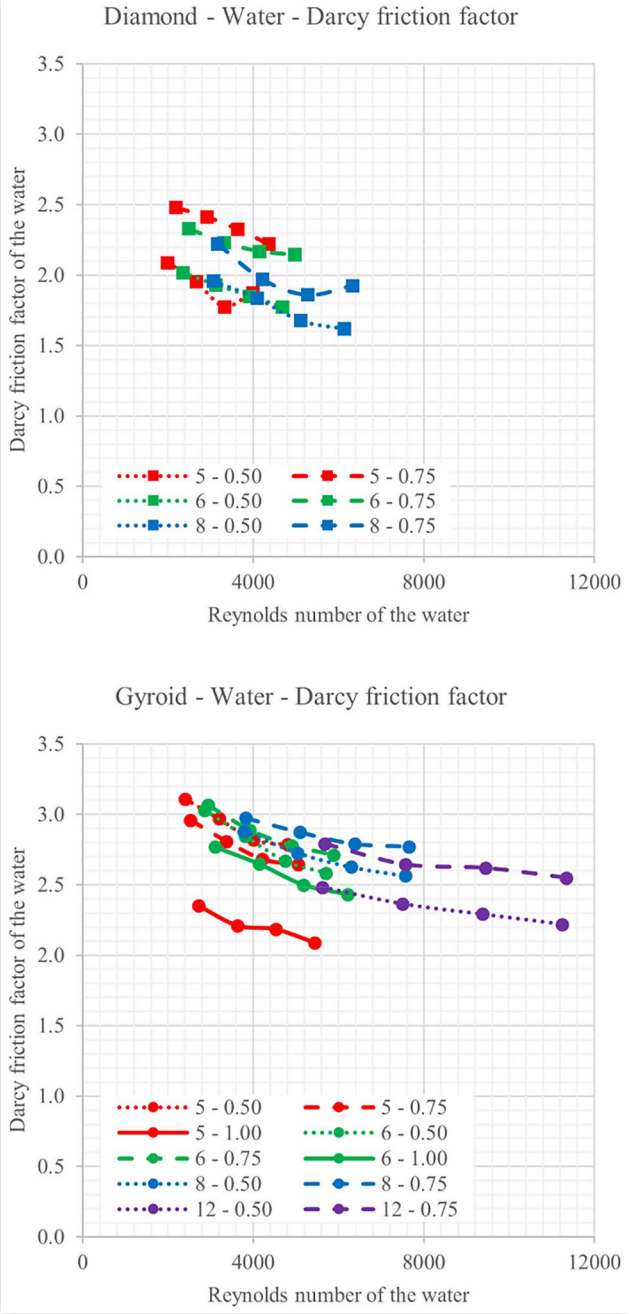

FIGURE 14 Darcy friction factor of oil for different TPMS topologies, unit cell sizes and wall thicknesses. Legend: unit cell size *l* [mm] – wall thickness *t* [mm].

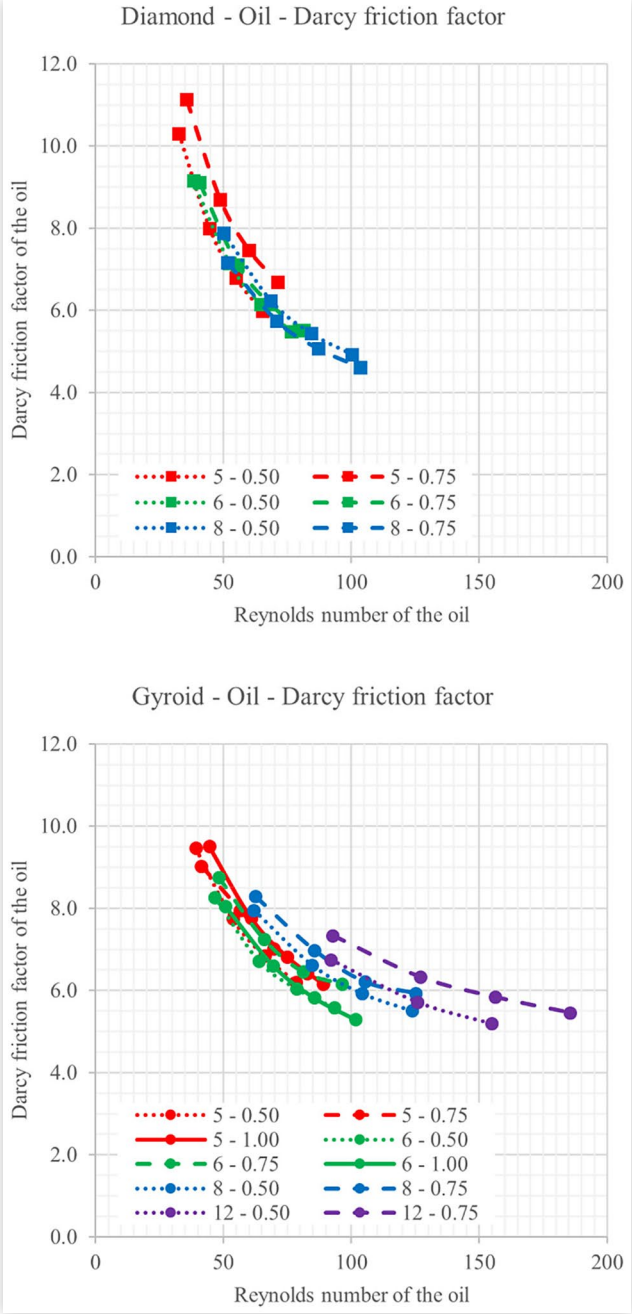

Downloaded from SAE International by Universita degli Studi di Modena, Wednesday, October 08, 2025

It is evident that the friction factor depends on the Reynolds number when the flow rate is increased in a certain geometry, excluding the possibility of a fully turbulent flow. It is not even laminar as the friction factor does not scale with 1/*Re*. However, it is interesting to notice that the friction factors associated with the Diamond structure are generally lower than those of the Gyroid. Nevertheless, this does not imply lower pressure drops because, considering Equation 29, the Diamond geometry generally has greater wall relative surface area and lower porosity than the Gyroid. Additionally, the friction factors change (instead of being perfectly overlapped) depending on the geometric parameters of the TPMS structure, but there is not a clear trend with wall thickness or unit cell size. Probably, the Darcy's law is not able to account for all the phenomena happening inside the heat exchanger such as the effect of the external wall which surrounds the TPMS structure or the shape of the inlet and outlet channels. Moreover, the geometric parameters also affect the value of Reynolds number for which the transition from laminar to turbulent flow occurs. In other words, the Darcy's law is related to a specific geometry and changing it leads to a different correlation.

Moving to the thermal performance, Figure 15 shows the heat transfer achieved by the heat exchanger, based on the TPMS structure.

First of all, it can be noted that the Diamond structure is generally characterized by higher heat transfer than the Gyroid. Indeed, the former has greater wall surface area and lower porosity than the former, as already shown in Figure 5. The heat transfer is proportional to the wall surface area, while a lower porosity means higher velocities, and convection, inside the TPMS channels, for a given flow rate. In order to separate the heat transfer from the effects of wall surface area and temperature difference between hot and cold fluids, the thermal performance of the heat exchanger is expressed in terms of global heat transfer coefficient in Figure 16.

Even in this case, the Diamond outperforms the Gyroid on equal unit cell size and wall thickness. For a fairer comparison, it is useful to consider the porosity of the structure (previously reported in Figure 5). As an example, at the maximum flow rate, the Diamond with 5 mm unit cell size and 0.75 mm wall thickness has ϕ = 0.472 and a global heat transfer coefficient equal to 2064 W/m^{2}K, while the Gyroid with 5 mm unit cell size and 1.00 mm wall thickness has ϕ = 0.462 (so roughly the same) and a global heat transfer coefficient of 1975 W/m^{2}K. Although, in this case, the Gyroid has slightly less porosity (i.e. higher velocity inside the channels) than the Diamond, the latter is still able to transfer more heat.

Following similar considerations, heat transfer can be increased by a reduction of the unit cell size, but the same is not always true when the wall thickness is increased. Indeed, the structures with high unit cell size (i.e. 8 and 12 mm) show a slightly reduction of heat transfer when the wall thickness is increased from 0.50 mm to 0.75 mm, while the opposite is true when the unit cell size is low (i.e. 5 or 6 mm). A higher wall thickness is associated to more conductive thermal resistance, lower

FIGURE 15 Heat transfer of the heat exchanger for different TPMS topologies, unit cell sizes, and wall thicknesses. Legend: unit cell size *l* [mm] – wall thickness *t* [mm].

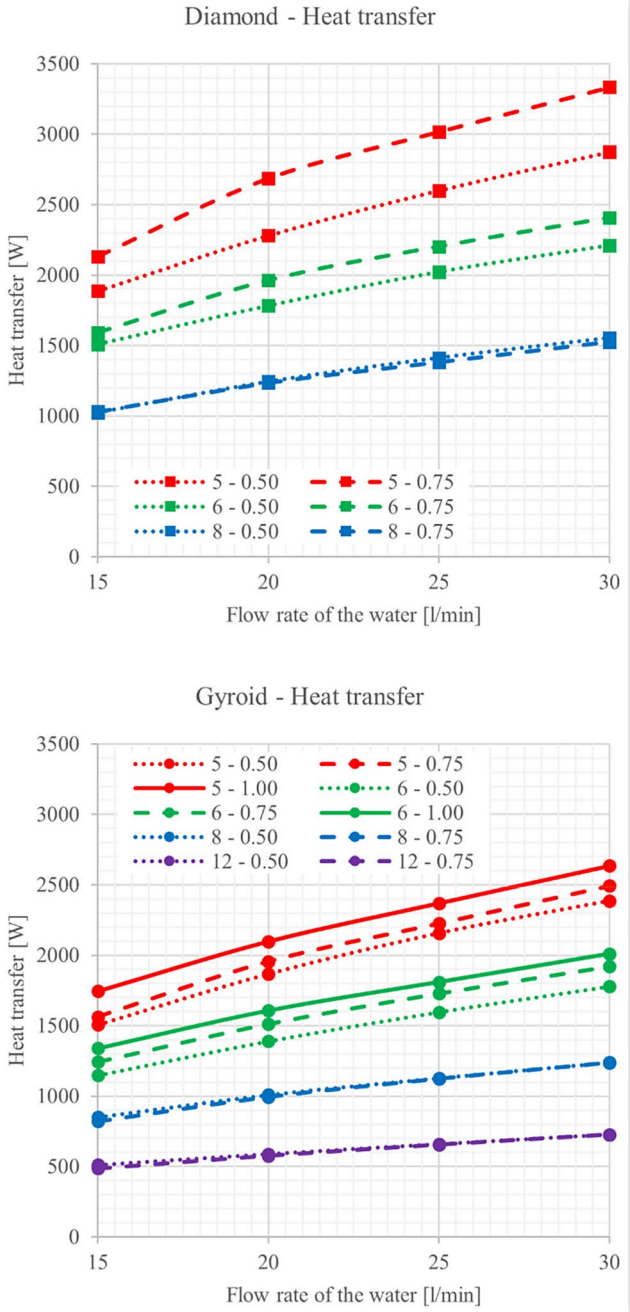

porosity (i.e. higher velocity and convection) and slightly lower wall surface area (i.e. lower heat transfer).

Given the contrasting effects of a wall thickness change on the thermal performance of the heat exchanger, it is useful to reason in terms of thermal resistance. Figure 17 presents convective, conductive and total thermal resistances for the Gyroid structures with 5 mm and 12 mm unit cell size, and different wall thickness. Firstly, the thermal resistance associated with the oil convection is significantly higher. Indeed, it represents more than 90% of the total resistance, due to high viscosity and low

Downloaded from SAE International by Universita degli Studi di Modena, Wednesday, October 08, 2025

FIGURE 16 Global heat transfer coefficient of the heat exchanger for different TPMS topologies, unit cell sizes, and wall thicknesses. Legend: unit cell size *l* [mm] – wall thickness *t* [mm].

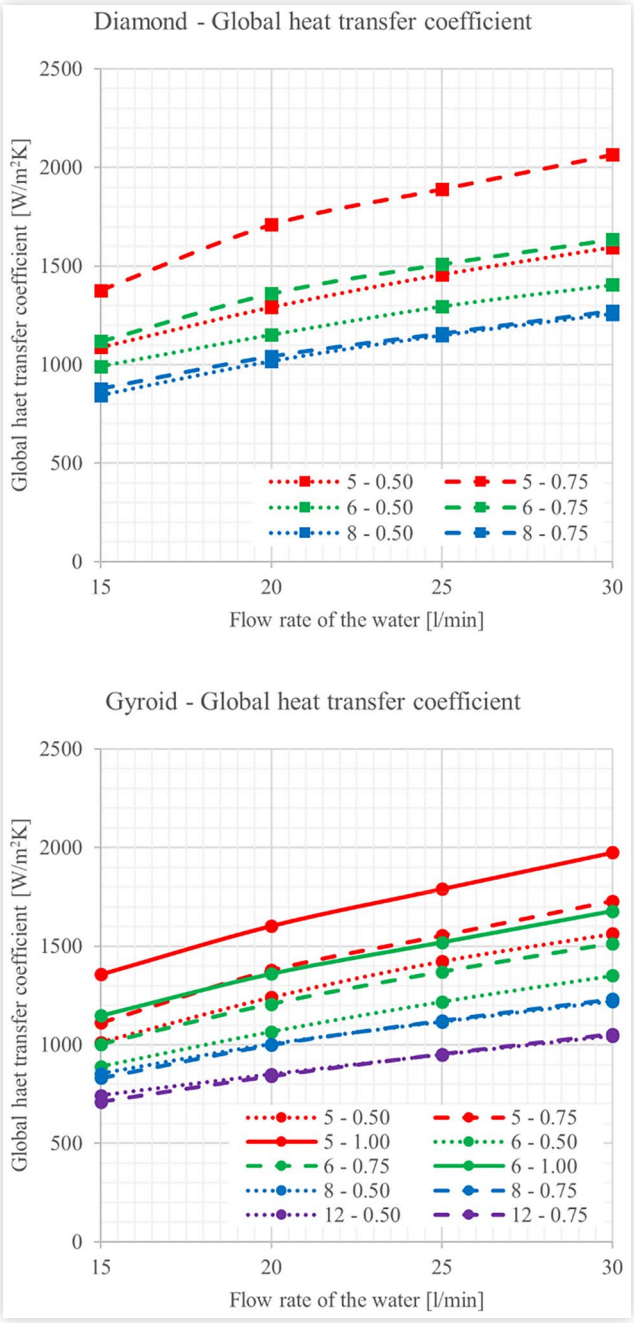

FIGURE 17 Thermal resistances of water (W), oil (O), solid (S), and overall (T) of the Gyroid structure for different unit cell sizes (5 mm and 12 mm) and wall thicknesses. Legend: wall thickness [mm] - water (W), oil (O), solid (S), overall (T).

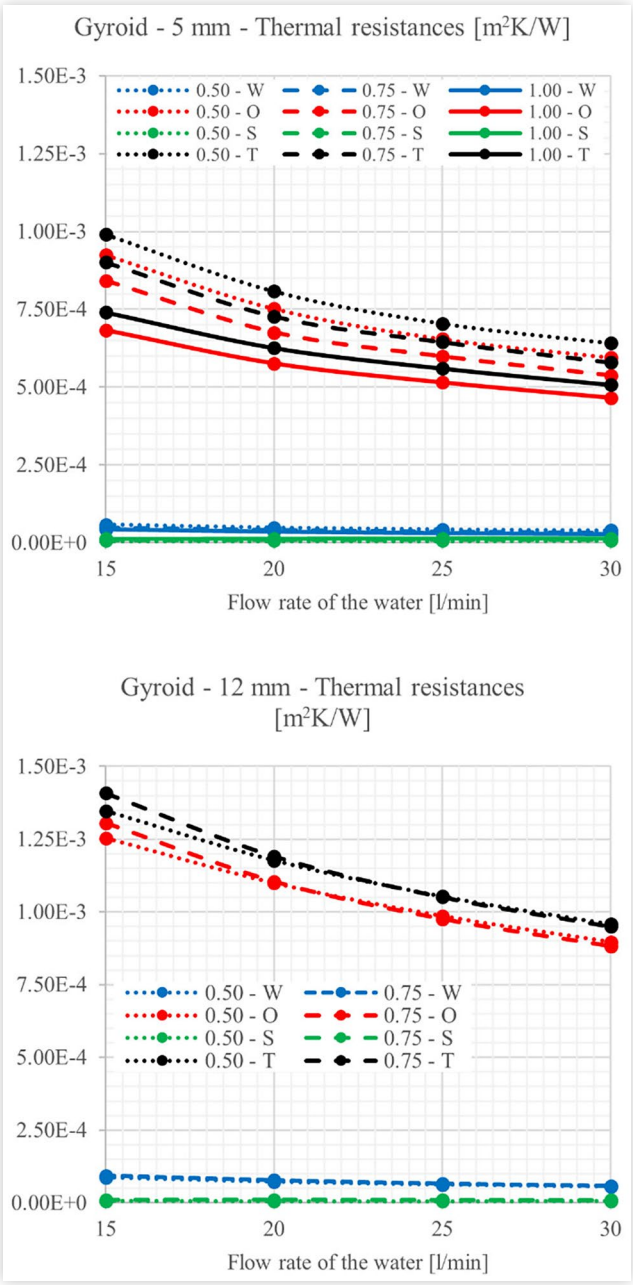

thermal conductivity of the oil, which together result in a very high Prandtl number compared to the water (as reported in Table 1). Consequently, when the wall thickness is modified, its main effect is on the heat convection of the oil side. In the case of small cells (e.g., 5 and 6 mm), a thickened wall is able to sufficiently increase the speed and the mixing inside the oil channel, reducing the convective thermal resistance. For larger cells (e.g. 8 and 12 mm), the effect is negligible. It is worth noting that a thickened wall also leads to greater convection on the water side and lower conduction through the solid, but such modifications are negligible and do not sensibly affect the overall performance of the heat exchanger.

To conclude the investigation on the thermal performance of the heat exchanger, the Nusselt number is plotted against the Reynolds number in Figure 18 and Figure 19, for water and oil, respectively. Consequently, it is possible to formulate correlations between Nusselt, Reynolds and Prandtl numbers in the form proposed in Equation 30.

$$Nu = CRe^{m}Pr^{n} \tag{30}$$

Downloaded from SAE International by Universita degli Studi di Modena, Wednesday, October 08, 2025

FIGURE 18 Nusselt number of the water for different TPMS topologies, unit cell sizes, and wall thicknesses. Legend: unit cell size *l* [mm] – wall thickness *t* [mm]. "Trend" refers to the Nusselt number correlation.

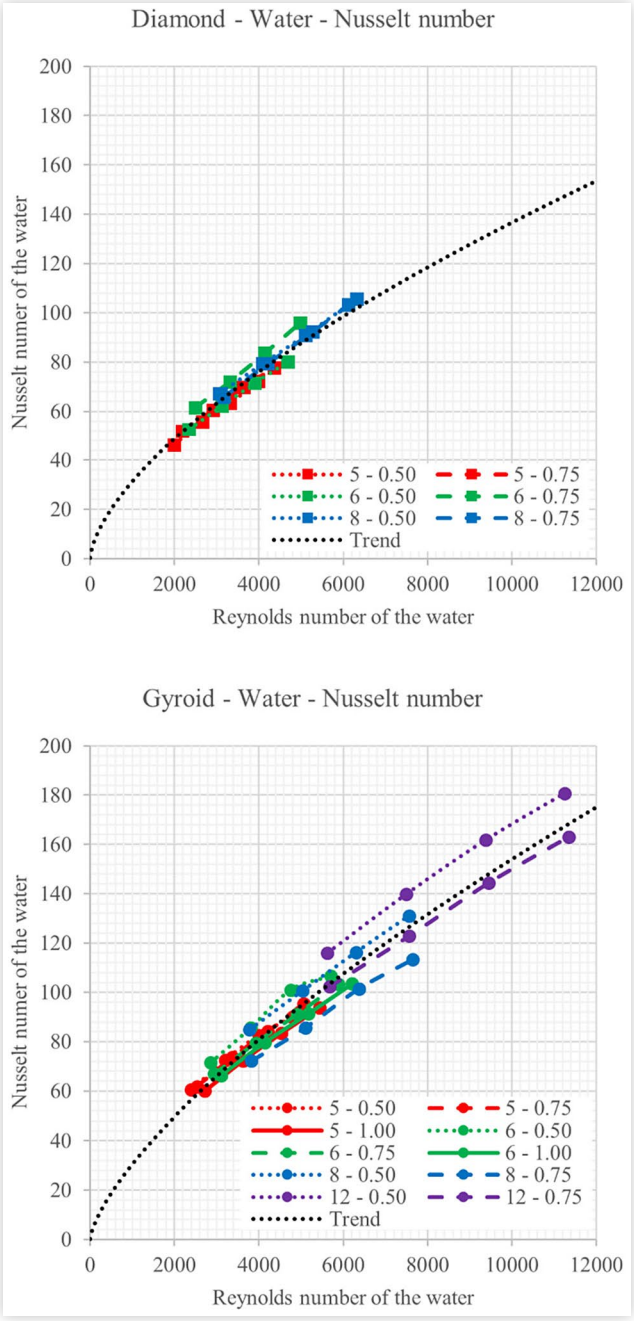

FIGURE 19 Nusselt number of the oil for different TPMS topologies, unit cell sizes, and wall thicknesses. Legend: unit cell size *l* [mm] – wall thickness *t* [mm]. "Trend" refers to the Nusselt number correlation.

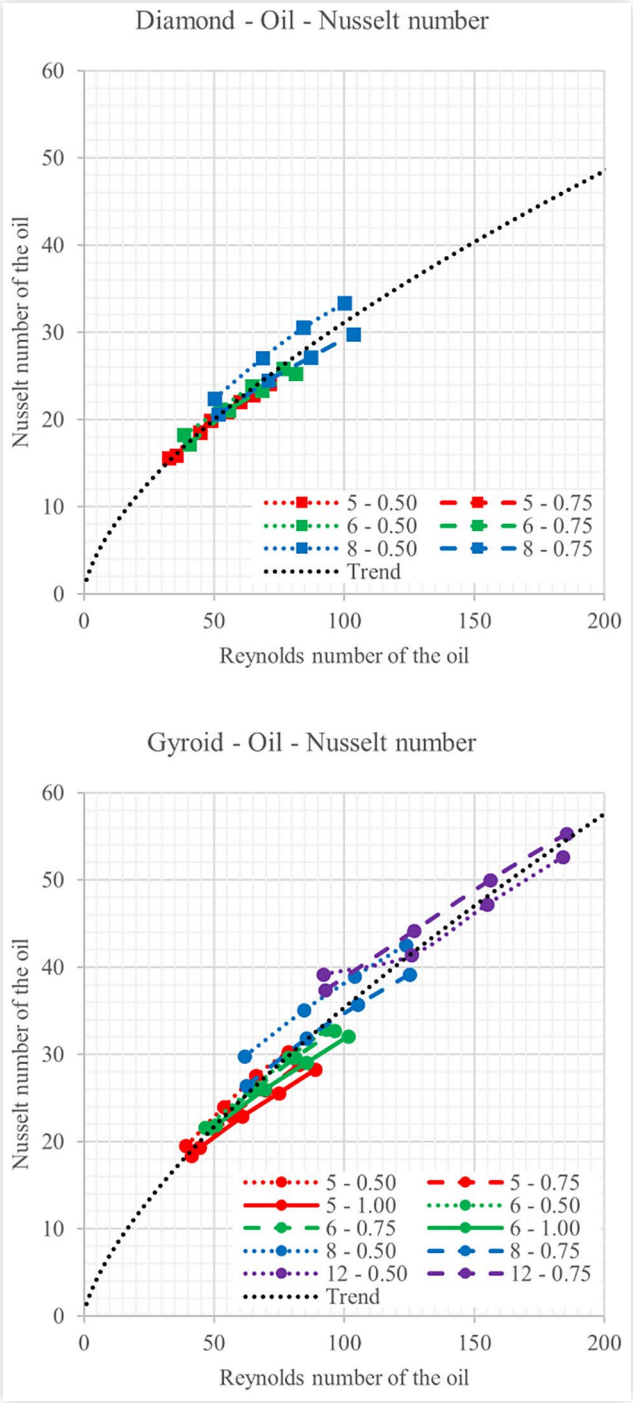

Downloaded from SAE International by Universita degli Studi di Modena, Wednesday, October 08, 2025

For the Diamond, the correlation can be expressed as in Equation 31.

$$Nu = 0.255Re^{0.640}Pr^{0.328} \quad (\sigma = 0.048) \tag{31}$$

For the Gyroid, the correlation is given by Equation 32.

$$Nu = 0.148Re^{0.704}Pr^{0.395} \quad (\sigma = 0.069) \tag{32}$$

σ is the standard deviation of the data with respect to the correlation.

For the design of a heat exchanger, it is of paramount importance to find the right balance between heat transfer and pressure drops. It is well known that increasing the flow rates of the fluids leads to higher heat transfer and pressure drops inside the heat exchanger, but there often are design constraints on these values due to, for example, energy consumption considerations or integration into a larger a system. Figure 20 compares heat transfer and total pumping power for all the combinations of TPMS topology, unit cell size and wall thickness.

Firstly, as expected, the heat transfer increases with the pumping power, while the efficiency decreases. In that sense, the heat exchanger is more efficient when the flow rates are low. Secondly, when compared on equal pumping power, heat transfer is always enhanced by smaller unit cell size and wall thickness. Lastly, the Diamond structure outperforms the Gyroid, as it is characterized by higher heat transfer on equal pumping power, at least for the investigated ranges of unit cell size and wall thickness.

FIGURE 20 Heat transfer against total pumping power of the heat exchanger for different TPMS topologies, unit cell sizes, and wall thicknesses. Legend: unit cell size *l* [mm] – wall thickness *t* [mm].

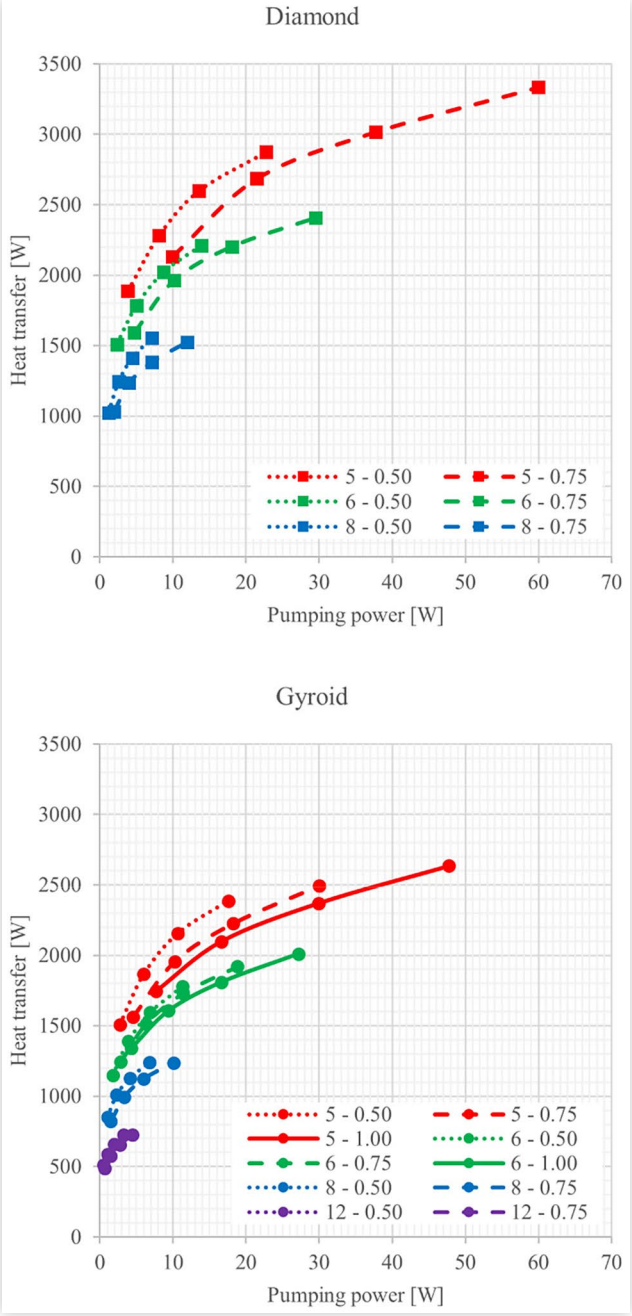

Conclusion

This study has explored the influence of geometric parameters, specifically unit cell size and wall thickness, on the thermo-fluid dynamic performance of TPMS-based heat exchangers for automotive applications. The investigation focuses on both Diamond and Gyroid lattice structures to be adopted as an automotive oil cooler.

The numerical CHT simulations were conducted by a CFD framework based on the Reynolds Stress Transport (RST) Elliptic Blending turbulence model and they revealed key aspects:

- The unit cell size is a critical design variable: reducing it leads to a higher heat transfer due to an increased area-to-volume ratio but also results in a significant rise in pressure drop.
- Wall thickness impacts both flow and thermal performance: increasing the wall thickness raises pressure losses and modifies heat transfer. However, its effect on thermal efficiency is variable. In small unit cell structures, thicker walls enhance convective heat transfer by accelerating the oil flow, while in larger unit cells, this benefit evanishes.
- Topology matters: the Diamond structure consistently outperformed the Gyroid in both heat transfer and flow resistance, achieving higher global heat transfer coefficients and greater heat transfer on equal pumping power.
- Thermal resistance analysis showed that the dominant limitation to heat transfer is on the oil side, due to the high Prandtl number. Therefore, geometric optimizations that enhance oil-side convection have the greatest impact on the overall performance.

Downloaded from SAE International by Universita degli Studi di Modena, Wednesday, October 08, 2025

Performance trade-offs are evident: smaller cells and thinner walls boost thermal efficiency but at the cost of higher pressure drops. A careful balance depending on the specific application is necessary.

Finally, empirical correlations between Nusselt number, Reynolds number and Prandtl number were derived for both Diamond and Gyroid structures, providing practical tools for preliminary design estimations.

Overall, these findings demonstrate that TPMS structures, particularly the Diamond topology, offer substantial opportunities for the development of compact, lightweight and efficient heat exchangers in high-performance automotive systems. The future work will focus on experimental validation of these results.

References

1. Arie, M., Shooshtari, A., and Ohadi, M., "Experimental Characterization of an Additively Manufactured Heat Exchanger for Dry Cooling of Power Plants," *Appl Therm Eng* 129 (2018): 187-198, doi:10.1016/J.APPLTHERMALENG.2017.09.140.
2. Li, X. and Tu, J., "Heat Exchangers in the Built Environment," *Sci Technol Built Environ* 25 (2019): 515, doi:10.1080/23744731.2019.1616963.
3. Culha, O., Gunerhan, H., Bıyık, E., Ekren, O. et al., "Heat Exchanger Applications in Wastewater Source Heat Pumps for Buildings: A Key Review," *Energy Build* 104 (2015): 215-232, doi:10.1016/J.ENBUILD.2015.07.013.
4. Abdelkareem, M.A. et al., "Heat Pipe-Based Waste Heat Recovery Systems: Background and Applications," *Thermal Science and Engineering Progress* (2022), doi:10.1016/j.tsep.2022.101221.
5. Witry, A., Al-Hajeri, M., and Bondok, A., "Thermal Performance of Automotive Aluminium Plate Radiator," *Appl Therm Eng* 25 (2005): 1207-1218, doi:10.1016/J.APPLTHERMALENG.2004.09.005.
6. Saltzman, D. et al., "Design and Evaluation of an Additively Manufactured Aircraft Heat Exchanger," *Appl Therm Eng* (2018), doi:10.1016/J.APPLTHERMALENG.2018.04.032.
7. Alteneiji, M., Ali, M., Khan, K.A., and Al-Rub, R., "Heat Transfer Effectiveness Characteristics Maps for Additively Manufactured TPMS Compact Heat Exchangers," *Energy Storage and Saving* (2022), doi:10.1016/j.enss.2022.04.005.
8. Careri, F., Khan, R., Todd, C., and Attallah, M., "Additive Manufacturing of Heat Exchangers in Aerospace Applications: A Review," *Appl Therm Eng* (2023), doi:10.1016/j.applthermaleng.2023.121387.
9. Du, W., Yu, W., France, D., Singh, M. et al., "Additive Manufacturing and Testing of a Ceramic Heat Exchanger for High-Temperature and High-Pressure Applications for Concentrating Solar Power," *Solar Energy* (2022), doi:10.1016/j.solener.2022.03.046.
10. Arie, M., Hymas, D., Singer, F., Shooshtari, A. et al., "An Additively Manufactured Novel Polymer Composite Heat Exchanger for Dry Cooling Applications," *Int J Heat Mass Transf* 147 (2020): 118889, doi:10.1016/j.ijheatmasstransfer.2019.118889.
11. Attarzadeh, R., Rovira, M., and Duwig, C., "Design Analysis of the "Schwartz D" Based Heat Exchanger: A Numerical Study," *Int J Heat Mass Transf* 177 (2021), doi:10.1016/j.ijheatmasstransfer.2021.121415.
12. Attarzadeh, R., Attarzadeh-Niaki, S.H., and Duwig, C., "Multi-Objective Optimization of TPMS-Based Heat Exchangers for Low-Temperature Waste Heat Recovery," *Appl Therm Eng* 212 (2022), doi:10.1016/j.applthermaleng.2022.118448.
13. Min, R., Wang, Z., Yang, H., Bao, R. et al., "Heat Transfer Characterization of Waste Heat Recovery Heat Exchanger Based on Flexible Hybrid Triply Periodic Minimal Surfaces (TPMS)," *International Communications in Heat and Mass Transfer* 157 (2024), doi:10.1016/j.icheatmasstransfer.2024.107760.
14. Abdelqader, O., Abu Al-Rub, R.K., and Hassan Ali, M.I., "Atmospheric Air Freshwater Using TPMS Compact Heat Exchangers," *Appl Therm Eng* 246 (2024), doi:10.1016/j.applthermaleng.2024.122979.
15. Abdelqader, O., Ali, K., Abu Al-Rub, R.K., and Hassan Ali, M.I., "Comparative Study of Finned Tube Geometries and TPMS Heat Exchangers for Enhanced Freshwater Production in Humid Environments," *International Journal of Thermofluids* 27 (2025), doi:10.1016/j.ijft.2025.101190.
16. Song, N., Pu, W., Qiao, L., Wu, B. et al., "Numerical Simulation Study on the Heat Transfer and Flow Characteristics of Fuel/Lubricating Oil Heat Exchanger Based on Triply Periodic Minimal Surface (TPMS)," *Appl Therm Eng* 257 (2024), doi:10.1016/j.applthermaleng.2024.124437.
17. Wang, H.C. et al., "Influences of the Flow Rate and Fluid Volume in Air-Kerosene Cross-Flow Heat Exchangers Using Gyroid-Typed Triply Periodic Minimal Surfaces," *Appl Therm Eng* 263 (2025), doi:10.1016/j.applthermaleng.2024.125336.
18. Torri, F. et al., "Evaluation of TPMS Structures for the Design of High Performance Heat Exchangers," SAE Technical Paper 2023-24-0125 (2023), doi:10.4271/2023-24-0125.
19. Al-Ketan, O. and Abu Al-Rub, R.K., "MSLattice: A Free Software for Generating Uniform and Graded Lattices Based on Triply Periodic Minimal Surfaces," *Material Design & Processing Communications* 3, no. 6 (2021): e205, doi:https://doi.org/10.1002/mdp2.205.
20. Tauzia, X., Maiboom, A., Karaky, H., and Chesse, P., "Experimental Analysis of the Influence of Coolant and Oil Temperature on Combustion and Emissions in an Automotive Diesel Engine," *International Journal of Engine Research* 20 (2019): 247-260, doi:10.1177/1468087417749391.
21. Siemens Digital Industries Software, "Simcenter STAR-CCM+," 2023, Siemens 2023.
22. Manceau, R. and Hanjalić, K., "Elliptic Blending Model: A New Near-Wall Reynolds-Stress Turbulence Closure," *Physics of Fluids* 14, no. 2 (2002): 744-754, doi:10.1063/1.1432693ï.

Downloaded from SAE International by Universita degli Studi di Modena, Wednesday, October 08, 2025

23. Lardeau, S. and Manceau, R., "Computations of Complex Flow Configurations Using a Modified Elliptic-Blending Reynolds-Stress Model," in *10th International ERCOFTAC Symposium on Engineering Turbulence Modelling and Measurements*, Marbella, Spain, 2014, https://hal.science/hal-01051799v1

24. Dixit, T., Al-Hajri, E., Paul, M.C., Nithiarasu, P. et al., "High Performance, Microarchitected, Compact Heat Exchanger Enabled by 3D Printing," *Appl Therm Eng* 210 (2022), doi:10.1016/j.applthermaleng.2022.118339.

Appendix A

The results of the mesh sensitivity analysis are presented. Figure 21 shows the tested meshes for each TPMS geometry, while Table 3 shows the main parameters of the selected meshes.

FIGURE 21 Mesh sensitivity analysis for all the tested TPMS cells. The deviation is from the heavier mesh, for each case. In red, the selected meshes.

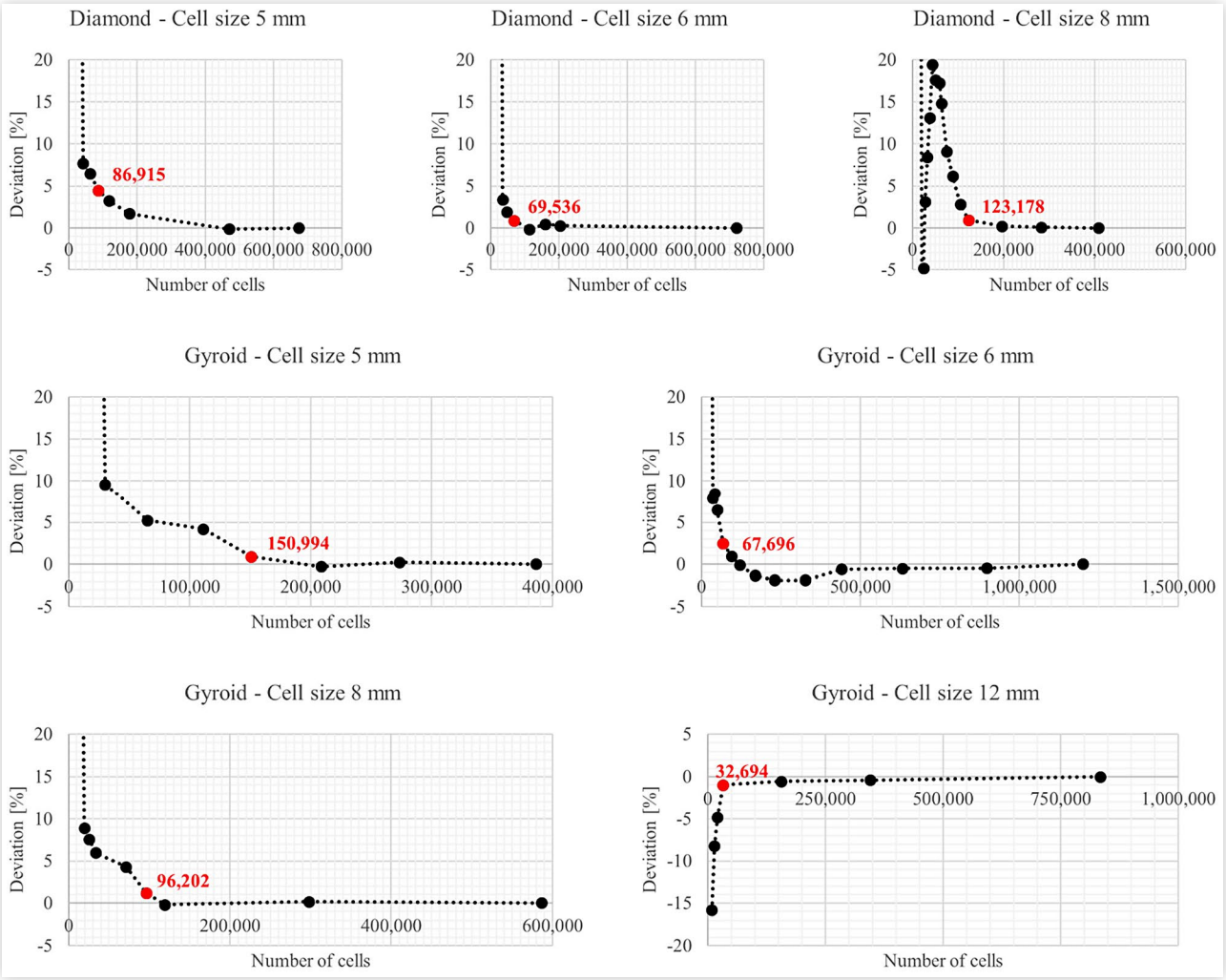

Downloaded from SAE International by Universita degli Studi di Modena, Wednesday, October 08, 2025

TABLE 3 Main parameters of the selected meshes.

Topology	Unit cell size mm	Thickness mm	Number of mesh cells -	Mesh cell size mm	Number of prism layers -	Stretch factor -	Near wall layer thickness μm	Average wall y^+ -
Diamond	5	0.75	86,915	0.100	8	1.47	4.5	0.97
Diamond	6	0.75	69,536	0.125	6	2.00	5.0	0.93
Diamond	8	0.75	123,178	0.267	8	1.50	5.9	1.03
Gyroid	5	0.75	150,994	0.078	8	1.50	3.0	1.02
Gyroid	6	0.75	67,696	0.133	8	1.50	5.2	1.13
Gyroid	8	0.75	119,446	0.136	8	1.50	5.3	1.24
Gyroid	12	0.75	32,694	0.400	8	1.50	10.0	1.06

© 2025 SAE International and SAE Naples Section. All rights reserved. No part of this publication may be reproduced, stored in a retrieval system, transmitted, in any form or by any means, electronic, mechanical, photocopying, recording, or otherwise, or used for text and data mining, AI training, or similar technologies, without the prior written permission of SAE.

Positions and opinions advanced in this work are those of the author(s) and not necessarily those of SAE International. Responsibility for the content of the work lies solely with the author(s).

ISSN 0148-7191